INTERNATIONAL JOURNAL FOR NUMERICAL METHODS IN FLUIDS, VOL. 21, 763–780 (1995)

THE INSTABILITY OF JETS OF ARBITRARY EXIT GEOMETRY

ROY S. BATY

Aerosciences and Fluid Dynamics Department, Sandia Laboratories, Albuquerque, NM 87185, U.S.A.

AND

PHILIP J. MORRIS

Department of Aerospace Engineering, The Pennsylvania State University, University Park, PA 16802, U.S.A.

SUMMARY

This paper describes a calculation technique to determine the linear instability characteristics of jets of arbitrary exit geometry. In particular, elliptic and rectangular jets are considered. The numerical procedure involves both a conformal transformation between the computational domain and the physical plane and a solution of the transformed stability equation in the computational domain. Modern, efficient, conformal mappings are used for both simply and doubly connected domains. The numerical solution is based on a hybrid finite difference/pseudospectral discretization of the stability equation. The technique is validated by comparison with previous stability calculations for circular and elliptic jets. Calculations are performed for the stability characteristics of elliptic and rectangular jets of aspect ratio 2:1. Growth rates, phase velocities, and pressure eigenfunctions are presented.

1. INTRODUCTION

This study is motivated by the authors' interest in turbulent mixing in free shear flows. It is now generally acknowledged that the mixing process in turbulent free shear flows is dominated by the dynamics of the large scale coherent structures. In addition, the local properties of these structures may be modelled by a linearized, inviscid analysis. The ability of a linear model to describe the local amplitude and phase variations of the large scale structures has been demonstrated in the experiments and analysis of excited free shear layers and jets by Gaster, Kit and Wygnanski[1] and Petersen and Samet[2]. Tam and Morris[3,4] made use of instability wave models of the large scale structures to predict the noise radiation from supersonic shear layers and the development of excited jets. In addition, Morris et al.[5] and Liou and Morris[6] and have developed Reynolds stress closure schemes in which the unknown turbulent stresses are described by solutions of the local linear stability equation. In these several models a knowledge of the properties of the instability wave leads to an understanding of the evolution of the large scale turbulent structures. For example, in the case of the supersonic jet noise model, the instability wave growth rate determines the amplitude evolution of an instability wave of a particular frequency. The real part of the wavenumber of the wave determines its spatial periodicity and phase velocity. If the phase velocity of the wave is supersonic with respect to the ambient speed of sound then a very efficient noise radiation called Mach wave radiation occurs.

The present paper is concerned with the instability of jets of arbitrary cross section. This analysis is an essential component in the extension of the models and analyses of turbulent flows described above to more complex geometries. Non-circular jets have been observed to have enhanced mixing properties

CCC 0271–2091/95/090763–18

Received 11 February 1993
Revised 18 April 1995

compared to circular jets. This makes their use attractive as injectors in combusters or as noise reduction devices in supersonic jets. For example, Gutmark *et al.*[7] demonstrated this enhanced mixing by the use of an elliptic jet in a dump combuster. In addition, rectangular and non-circular jets have applications in thrust vectoring/thrust-reversing engine nozzles for future fighter aircraft.

In this paper a hybrid numerical scheme is developed to calculate the eigenvalues of the spatial stability problem associated with jets of arbitrary exit geometry. The computational scheme presented here generalizes existing numerical methods for the jet stability problem in the sense that it is applicable directly to any non-circular jet exit geometry. Calculations of the stability characteristics of non-circular jets have been made previously by several authors. Morris[8] considered an elliptic jet with a mean velocity profile chosen in such a way that the stability equation was separable. Koshigoe and Tubis[9,10] also considered an elliptic jet. Their latter paper most closely resembles the present approach in that it used a generalized shooting method. However, an integral formulation was used to establish the conditions at the edges of the jet shear layer. Also, the discretization in the azimuthal direction needed far more points than the spectral approach used in the present scheme. Finally, they only considered thin shear layers. Tam and Thies[11] studied the instability of rectangular jets. They used a boundary integral method to consider jets represented by a vortex sheet. The present method is applicable to jets with realistic velocity and density profiles.

The hybrid scheme developed here is used in a study of the stability characteristics of both elliptic and rectangular jets. These characteristics are given in the form of the variation of the growth rates and phase velocities as a function of the instability wave frequency. In addition, the eigenfunctions for the most unstable modes are also shown. The development of the hybrid method is outlined using a model partial differential equation which has an exact analytic solution. In general, the hybrid method developed here is applicable to linear, elliptic, two-dimensional, partial differential equations of the form:

$$\sum_{|\beta| \le k} \alpha^{\beta} \; a_{\beta} \; \partial^{\beta}(\phi) = 0, \tag{1}$$

where α is an unknown eigenvalue, ϕ is an unknown eigenfunction, and β is a multi-index. Equation (1) is defined on some planar domain Ω with the boundary conditions:

$$\phi\,(x, y) \text{ defined on } \partial\Omega \tag{2}$$

In the present paper we first develop the hybrid numerical scheme. A generalized Rayleigh equation that governs the inviscid, incompressible, spatial stability of arbitrary geometry shear flows is then described. Then a model problem is introduced to help in the development and description of the numerical solution technique. This scheme is then applied to the generalized Rayleigh equation. Finally, calculations are performed for the stability characteristics of elliptic and rectangular jets.

2. HYBRID NUMERICAL SCHEME

This section develops a hybrid numerical scheme to solve linear, elliptic eigenvalue problems of the form given by equation (1). Hybrid techniques are numerical methods that combine series approximations with finite difference calculations. For two-dimensional partial differential equations, such as the equation governing the inviscid stability of non-circular jets, hybrid methods generate discretization matrices whose order varies linearly with the approximating series summation bound, N. This implies that the number of operations required to compute an eigenvalue of equation (1) is $O(N^3)$. This estimate is an improvement over the number of operations required by full spectral or pseudospectral methods. Such series techniques generate discretization matrices from two-dimensional

series approximations whose size is $O\{(N+1)^2\}$. This implies that such methods require $O\{(N+1)^6\}$ operations to compute an eigenvalue for a standard two-dimensional problem. Furthermore, hybrid techniques have the advantage of increased accuracy over purely finite difference approaches. The accuracy of a hybrid scheme depends on the properties of the approximating series and on the accuracy of the finite difference scheme. The present study uses a pseudospectral series and a fourth-order Runge–Kutta scheme. The use of a pseudospectral series assumes that the function to be approximated is known, or may be computed, on a fixed set of points in the computational domain. This information is then used with an appropriate set of basis functions to form a finite series approximating the function. The function's approximation on a known set of points defines a grid in the computational domain.

2.1. The Generalized Rayleigh Equation

Consider a jet flow issuing from a nozzle of arbitrary cross-section. The governing equations will be developed in a Cartesian co-ordinate system (x, y, z). The axis of the jet is aligned with the z axis and the basic axial velocity is denoted by $W(x, y)$. The mean velocity components in the x and y directions are neglected. This is the parallel flow approximation of hydrodynamic stability. If the parallel flow approximation is not used and the small effects of the divergence of the basic flow are to be considered, the problem may be solved with a multiple-scales analysis (see reference 12). The parallel flow solution is then the lowest-order approximation; however, the effects of flow divergence are not included in the present study.

A linear, elliptic, partial differential for the pressure may be obtained by taking the divergence of the momentum equation and by use of the equation of continuity. The resulting equation may be linearized about the basic flow. The velocity fluctuations are eliminated in favor of the pressure fluctuation using the linearized momentum equations. In the resulting equation the coefficients are functions of x and y only; thus, a separable solution for the pressure fluctuation $p(x, y, z, t)$ may be sought in the form,

$$p(x, y, z, t) = \hat{p}(x, y) \exp[\mathrm{i}(\alpha z - \omega t)], \tag{3}$$

where, α is the axial wavenumber and ω is the radian frequency. If solutions of the form (3) are substituted into the fluctuation pressure equation it becomes,

$$(\Delta - \alpha^2)\hat{p} + \frac{2\alpha}{\omega - \alpha W} \nabla W \cdot \nabla \hat{p} = 0. \tag{4}$$

Equation (4) is the non-separable form of the Rayleigh equation for inviscid, incompressible flow. In order to determine the fluctuation pressure $\hat{p}$ the boundary conditions must be specified. In the present case the pressure fluctuation is required to satisfy,

$$\hat{p} \to 0 \text{ as } r \to \infty \tag{5}$$

and

$$\hat{p} \text{ is finite as } r \to 0, \tag{6}$$

where r is the radial distance from the jet centreline.

To consider jets of arbitrary geometry, conformal mappings are used to map standard computational domains onto realistic jet flow cross sections. Conformal mapping is analytically a very desirable technique. Such maps simplify the governing differential equation by generating a diagonal metric tensor. Recently, very efficient schemes have been developed to determine the conformal maps from standard computational domains onto arbitrary regions in the plane. Wegmann[13–15] proposed a scheme to compute the conformal maps from canonical domains onto simply and doubly connected regions with smooth boundaries. This technique has been applied in the present paper to determine the co-

ordinate maps needed for an elliptic jet flow cross-section. For polygonal regions, Trefethen[16,17] has developed an efficient software package, SCPACK, to determine the conformal map and its inverse from the interior of a polygon onto the unit disc. In the present study, SCPACK has been applied to determine the conformal maps needed in the study of a rectangular jet flow cross section. The details of the conformal grid generation techniques are given by Baty[18]. To apply conformal maps, the Rayleigh problem must be recast in general conformal co-ordinates. Let Cartesian co-ordinates be denoted by (x^1, x^2), and let the computational co-ordinates be denoted by (y^1, y^2). Now, let f denote a conformal map satisfying the relations,

$$x^1 = Re\{f(y^1 + \mathrm{i}y^2)\} \tag{7}$$

and

$$x^2 = Im\{f(y^1 + \mathrm{i}y^2)\}. \tag{8}$$

If equations (7) and (8), the Cauchy–Riemann equations, and the general tensor form of equation (4) are used, the generalized Rayleigh equation in terms of (y^1, y^2) may be written

$$(\Delta - \hat{g}\alpha^2)\hat{p} + \frac{2\alpha}{\omega - \alpha W}\nabla W \cdot \nabla \hat{p} = 0, \tag{9}$$

where

$$\hat{g} = |f'(y^1 + \mathrm{i}y^2)|^2. \tag{10}$$

2.2. *The Model Problem*

To facilitate the development of a numerical scheme to solve eigenvalue problems of the form (1) and (10) a model problem with an exact solution has been used. Consider the following partial differential equation:

$$\Delta\phi - 2\alpha\omega\left(\frac{\partial\phi}{\partial x} + \frac{\partial\phi}{\partial y}\right) + 2\alpha^2\phi = 0 \tag{11}$$

defined on the set Ω,

$$\Omega := [(x, y) \in \mathbf{R}^2 | -1 \leq x, y \leq 1], \tag{12}$$

with the boundary conditions

$$\phi = 0 \quad \text{on} \quad \partial\Omega. \tag{13}$$

In equation (11) α represents a complex parameter and ω is a fixed real parameter analogous to the wavenumber and frequency respectively in the Rayleigh equations (4) or (9). The main difference between the model equation and the Rayleigh equation is that the former has constant coefficients. This yields a simple separable solution of the form,

$$\phi(x, y) = \sum_{n=1}^{\infty}\sum_{m=1}^{\infty} \phi_{nm} \exp[\alpha\omega(x + y)]\psi_n(x)\psi_m(y), \tag{14}$$

where

$$\psi_k(\xi) = \begin{cases} \sin\left(\frac{1}{2}\pi k\xi\right) & k \text{ is even}, \\ \cos\left(\frac{1}{2}\pi k\xi\right) & k \text{ is odd}. \end{cases} \tag{15}$$

Here, ξ represents either x or y. Furthermore, the exact dispersion relationship is given by

$$\alpha = \pm i\sqrt{\frac{(n^2+m^2)\pi^2}{8(\omega^2-1)}} \text{ for } n, m = 1, 2, 3, \ldots . \tag{16}$$

The results from the numerical method developed below to solve this model eigenvalue problem will be compared to the first three distinct eigenvalues computed from equation (16), for the frequency, $\omega = 2{\cdot}0$.

$$\begin{aligned} \alpha_1 &= \pm 0{\cdot}9068996i, \\ \alpha_2 &= \pm 1{\cdot}4339343i, \\ \alpha_3 &= \pm 1{\cdot}8137993i. \end{aligned} \tag{17}$$

2.3. *Numerical Solution of the Model Problem*

The hybrid method presented here is defined using a pseudospectral series based on the Chebyshev polynomials. The details of the pseudospectral technique for a one-dimensional problem are given by Voigt *et al.*[19] To outline the method, consider the model equation (11). Assume that the function to be approximated may be represented in a series of the form:

$$\phi(x, y) \approx \sum_{i=0}^{N} a_i(y) f_i(x). \tag{18}$$

In equation (18), the coefficients $a_i(y)$, are functions of the grid points defined by

$$x_j = \cos(\pi j/N) \text{ for } j = 0, 1, 2, \ldots, N. \tag{19}$$

Moreover, the basis functions, f_i, are rational functions defined by

$$f_i(x) = \frac{(1-x)T'_N(x)(-1)^{i+1}}{c_i N^2 (x - x_i)}, \tag{20}$$

with

$$c_0 = c_N = 2 \tag{21}$$

and

$$c_j = 1 \quad \text{otherwise.} \tag{22}$$

Here, $T'_N(x)$ is the derivative of the Nth order Chebyshev polynomial. The evaluation of equation (20) at the grid points leads to the relation:

$$f_i(x_j) = \delta_{ij}, \tag{23}$$

where δ_{ij} is the Kronecker delta. Equation (23) is the result that allows the pseudospectral method to discretize a given boundary value problem efficiently. Next, if equation (18) is substituted into the model partial differential equation (11), we obtain:

$$\begin{aligned} \sum_{i=0}^{N} a_i(y) f_i''(x) + \sum_{i=0}^{N} a_i''(y) f_i(x) - 2\alpha\omega \left\{ \sum_{i=0}^{N} a_i(y) f_i'(x) + \sum_{i=0}^{N} a_i'(y) f_i(x) \right\} \\ + 2\alpha^2 \sum_{i=0}^{N} a_i(y) f_i(x) = 0, \end{aligned} \tag{24}$$

where primes denote ordinary derivatives. To simplify this equation, the derivatives of the approximating basis functions at the grid points must be determined. Voigt *et al.*[19] gives these derivatives as:

$$\left|\frac{d^p f_i(\xi)}{d\xi^p}\right|_{\xi=\xi_j} = (D^p)_{ji}, \tag{25}$$

where

$$(D^1)_{ji} = \frac{c_j(-1)^{i+j}}{c_i(\xi_j - \xi_i)} \quad \text{if} \quad j \neq i, \tag{26}$$

$$(D^1)_{jj} = \frac{-\xi_j}{2(1-\xi_j^2)}, \tag{27}$$

$$(D^1)_{00} = \frac{2N^2+1}{6} = -(D^1)_{NN} \tag{28}$$

and

$$(D^p) = (D^1)^p. \tag{29}$$

Now, if equations (25)–(29), are used in equation (24) a system of linear, second-order ordinary differential equations in terms of the coefficients is produced:

$$a_k''(y) - 2\alpha\omega a_k'(y) + 2\alpha^2 a_k(y) + \sum_{i=0}^{N} a_i(y)(D^2)_{ki} - 2\alpha\omega \sum_{i=0}^{N} a_i(y)(D^1)_{ki} = 0. \tag{30}$$

Equation (30) is then recast as a first-order system. This system of first order equations can then be recast as a matrix equation with the unknown vector being the coefficients of the approximating series. The resulting matrix equation may be integrated once the boundary conditions are determined. In the pseudospectral direction, x, the boundary conditions are applied easily as they determine the values of the first and last coefficients in the series (18). The model eigenvalue problem has homogeneous boundary conditions that require that these coefficients in the approximating series are zero. In the finite difference direction, however, the boundary value problem is recast as an initial value problem in order to apply an explicit integration scheme. The boundary conditions are recast using a generalized shooting technique. Another example of such a method is given by Koshigoe *et al.*[10] in which an integral method is used to specify the conditions on the boundaries. The shooting technique is constructed by the introduction of the following initial conditions:

$$\frac{\partial}{\partial y}\sum_{i=0}^{N} a_i(y) f_i(x_j)\bigg|_{y=-1} = 1 \text{ for each } j, \tag{31}$$

$$a_i(-1) = 0. \tag{32}$$

The system of ordinary differential equations is then integrated to the boundary defined by $y = 1$ in the computational domain for each initial condition given in equations (31) and (32). The solution on $y = 1$ is then given by a linear sum of the integrated solutions:

$$\sum_{i=1}^{N-1} R_i \mathbf{V}(x_i), \tag{33}$$

where the integrated solutions are denoted by $\mathbf{V}(x_i)$ and the unknown coefficients by R_i. If the boundary condition at $y = 1$ is applied, that is,

$$\phi(x, 1) = 0, \tag{34}$$

a system of homogeneous simultaneous equations for the R_i is obtained. For a non-trivial solution for the coefficients R_i the determinant of the coefficient matrix must be zero, that is

$$\det[\mathbf{V}(x_1), \cdots, \mathbf{V}(x_{N-1})] = 0. \tag{35}$$

Recall that this matrix is an implicit function of the wave number, α. Only when α is an eigenvalue will equation (35) be satisfied. To determine the eigenvalues a local Newton–Raphson scheme is applied. All the numerical experiments have been performed using a fourth-order, Runge–Kutta integration scheme with various step sizes. The numerical results given in this section are for a step size $\Delta y = 0{\cdot}02$.

The hybrid method has been used to compute the first three distinct eigenvalues for the model problem with $\omega = 2{\cdot}0$. Table I shows the absolute errors for these eigenvalues. The numerical results show that the hybrid method works well in the approximation of the eigenvalues for the model problem. It is clear from Table I that to achieve a certain absolute level of accuracy for the higher eigenvalues a higher order spectral approximation is required. This is because the higher order eigensolutions are more oscillatory. Fortunately in the primary problem of interest, the jet stability problem, only the lowest order modes dominate the unsteady flow structure.

2.4. Discretization of the Generalized Rayleigh Problem

The discretization of the generalized Rayleigh problem follows the steps used for the model problem. Equation (18) is substituted into equation (9) and then equations (23) and equations (25–29) are used to generate a system of linear, second order ordinary differential equations in terms of the series coefficients:

$$\begin{aligned} a_k''(y^2) = \left\{\frac{2\alpha}{\omega - \alpha W}\right\} \frac{\partial W}{\partial y^2} a_k'(y^2) - \hat{g}\alpha^2 a_k(y^2) + \sum_{i=0}^{N} a_i(y^2)(D^2)_{ki} \\ + \left\{\frac{2\alpha}{\omega - \alpha W}\right\} \frac{\partial W}{\partial y^1} \sum_{i=0}^{N} a_i(y^2)(D^1)_{ki} = 0. \end{aligned} \tag{36}$$

Equation (36) is then recast as a matrix equation with the unknown vector containing the pseudospectral coefficients. The resulting matrix equation may be integrated once the boundary conditions are determined. In the region outside the jet mixing layer the velocity is taken to be zero. Then the Rayleigh equation reduces to the Helmholtz equation:

$$(\Delta - \hat{g}\alpha^2)\hat{p} = 0. \tag{37}$$

Table I. Absolute errors in the first three eigenvalues of the model problem

N	Abs. error 1	Abs. error 2	Abs. error 3
5	1·10(−2)	5·82(−1)	1·57(−1)
7	5·18(−5)	1·59(−3)	1·02(−1)
8	2·02(−5)	5·64(−4)	2·81(−2)
9	7·45(−7)	2·41(−5)	6·28(−3)

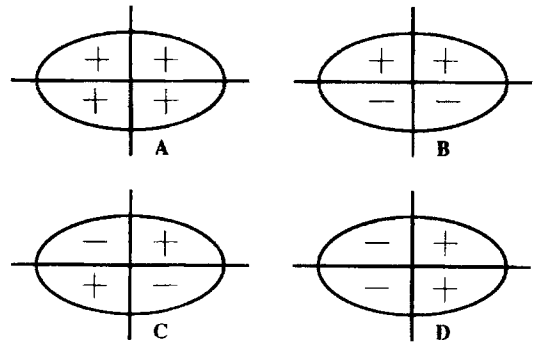

Figure 1. Sketch of the four classes of instability waves for elliptic and rectangular jets. A–D correspond to equations (40)–(43)

The general solution to equation (37) in polar co-ordinates that satisfies the boundary condition (5) may be written:

$$\hat{p}(r, \theta) = \sum_{n=0}^{\infty} A_n H_n^{(1)}(\mathrm{i}\alpha r) \exp(\mathrm{i} n \theta), \tag{38}$$

where, $H_n^{(1)}$ is the Hankel function of the first kind and order n. Moreover, since the pressure fluctuation must be bounded as $r \to 0$, then in the jet potential core it satisfies:

$$\hat{p}(r, \theta) = \sum_{n=0}^{\infty} B_n J_n(\mathrm{i}\alpha r) \exp(\mathrm{i} n \theta), \tag{39}$$

where J_n is the Bessel function of the first kind. This form of solution is appropriate in the annular jet mixing region upstream of the end of the jet potential core. Downstream of the potential core the solution on the jet centreline may be obtained from a Frobenius solution.

If the jet basic flow possesses any symmetries it is possible to classify the instabilities in a more specific way. For example, if the jet basic flow is symmetric about its major and minor axes, as would be the case for the elliptic and rectangular jets considered here, there are four classes of possible azimuthal pressure solutions. These four classes of solutions are shown schematically in Figure 1 for an elliptic jet. The infinite series describing these solutions may be written,

$$\sum_{n=0}^{\infty} A_n C_n(\mathrm{i}\alpha r) \cos(2 n \theta), \tag{40}$$

$$\sum_{n=0}^{\infty} A_n C_n(\mathrm{i}\alpha r) \sin[(2 n + 1)\theta], \tag{41}$$

$$\sum_{n=0}^{\infty} A_n C_n(\mathrm{i}\alpha r) \sin[(2 n + 2)\theta], \tag{42}$$

$$\sum_{n=0}^{\infty} A_n C_n(\mathrm{i}\alpha r) \cos[(2 n + 1)\theta], \tag{43}$$

where C_n represents either J_n or $H_n^{(1)}$. The azimuthal symmetries shown in Figure 1 correspond to the equations (40–43), respectively. Since the jet basic flow is assumed to be symmetric about both the major and minor axes the computation may be restricted to the first quadrant in the physical plane. The standard computational domain for this physical region is taken to be a rectangle. On the upper and

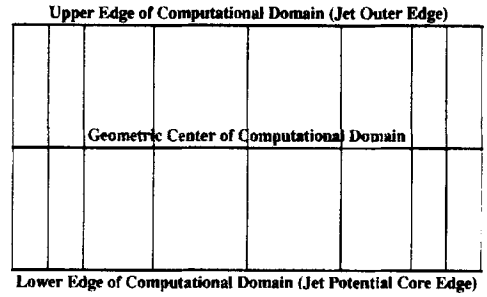

Figure 2. Example computational domain for the summation bound $N = 8$. The upper and lower edges of the computational domain correspond to the mean jet boundaries. The vertical lines correspond to the grid points for the pseudospectral approximation

lower edges of this domain that correspond to constant radial locations, the solutions take the forms given by equations (40)–(43). Before these boundary conditions are evaluated in the computational space they are transformed using the metric generated by the conformal mapping. On the side edges of the computational domain that represent the jets positive minor and major axes, the boundary conditions are determined by the symmetry conditions as sketched in Figure 1. If the pressure is odd about an axis the boundary condition may be written

$$\hat{p} = 0, \tag{44}$$

and if the fluctuation is even about an axis the boundary condition may be written

$$\frac{\partial \hat{p}}{\partial \theta} = 0. \tag{45}$$

The set of equations for the unknown series coefficients, equation (36), may be integrated explicitly in the radial direction once the boundary conditions have been converted into the appropriate initial conditions. The boundary conditions on the top and bottom edges of the computational domain are changed into initial conditions using the generalized shooting method as in the model problem. Let N denote the summation bound for the approximating series. Then there are $N - 1$ interior grid points in the 'azimuthal' y^1 direction. Figure 2 shows a sketch of a computational domain for $N = 8$. In this figure, the horizontal direction represents an azimuthal variation in the jet and the vertical direction represents the radial direction. On the lower edge of the computational domain, the first term and its derivative from the exact series solution as given by equation (39) are evaluated at the grid points. In Figure 2 these grid points are at the lower ends of the vertical lines. These values are used as the initial conditions on the lower boundary. The matrix containing the system of differential equations is then integrated to the geometric centre of the computational domain y_c, yielding $\mathbf{V}_1^l$, where

$$\mathbf{V}_1^l = [a_o^1(y_c), a_1^1(y_c), a_2^1(y_c), \cdots, a_N^1(y_c)]^{\mathrm{T}}, \tag{46}$$

where $a_k^j(y_c)$ denotes the value of the j-th coefficient on the line x_k at the position y_c. At each step in the explicit integration procedure the boundary conditions on the vertical edges of the computational domain are satisfied by solving for the first and last coefficients of the approximating series or its derivative.

On the upper edge of the computational domain, the first term in the exact series solution (38) and its derivative are evaluated at the grid points. The matrix containing the system of differential equations is then integrated to the centre computational domain, producing $\mathbf{V}_1^u$. This process of evaluating a term and its derivative from the exact series solution on the boundaries is repeated for each interior grid line

using $N-1$ terms from the exact series solutions on the horizontal edges of the computational domain. The resulting integrated solutions and their derivatives are then matched at the center of the domain. The matching is accomplished by requiring that a linear combination of the $2(N-1)$ solutions be equated to zero:

$$\sum_{i=1}^{N-1} (R_i \mathbf{V}_i^u + S_i \mathbf{V}_i^l) = 0. \tag{47}$$

For equation (47) to have a non-trivial solution the determinant of the matrix of integrated solutions must be zero. Recall that the solution vectors are implicit functions of a fixed real frequency and some complex wavenumber α. A Newton–Raphson scheme is used to locate the wavenumbers at which the determinant is zero.

Once the eigenvalue of the Rayleigh problem has been computed, its corresponding eigenfunction may be calculated. The hybrid method computes the linear solutions $\mathbf{V}_i^u$ and $\mathbf{V}_i^l$ as it integrates from the upper and lower edges of the shear layer to its geometric centre. However, the relative weights of the integrated solutions R_i and S_i are not known. These coefficients may be found by writing equation (47) in the form,

$$(\mathbf{V}_i^u, \mathbf{V}_i^l)\begin{pmatrix} R_i \\ S_i \end{pmatrix} = 0. \tag{48}$$

The coefficients are obtained by the inverse interpolation method, Stewart[20]. The generalized Rayleigh equation is then integrated a final time using the scaled initial conditions and the pseudospectral amplitudes, $a_i(y^2)$, are stored along each radial grid line. Thus, the eigenfunction is approximated discretely in the radial direction, and by a series in the azimuthal direction.

2.5. *The Mean Velocity Profile*

In general, if the mean velocity profile $W(x^1, x^2)$ is known in the physical co-ordinates, the conformal map may be used to describe the velocity profile and its derivatives in the computational plane. In the present calculations, for convenience, the mean velocity profile has been assumed to be a function of y^2 alone. This is the case for axisymmetric jets or for the elliptic jets considered by Morris[8] in which the mean velocity was assumed to be only a function of the 'radial co-ordinate' in an elliptic cylindrical co-ordinate system. In this case the velocity profiles were in reasonable agreement with experiments for thin shear layers.

The jet mean velocity profile used in the present calculations is based on a generalization of the profile given by Michalke[21] for a circular jet. This profile may be written,

$$W(y^2) = \begin{cases} 1, & 0 \le r < R - \frac{1}{2}\delta, \\ \frac{1}{2}\left\{1 + \tanh\left[\dfrac{R}{2\theta}\left(1 - \dfrac{r}{R}\right)\right]\right\}, & R - \frac{1}{2}\delta < r < \infty, \end{cases} \tag{49}$$

where R is the jet exit radius, θ is the momentum thickness and δ is chosen such that

$$\tanh(\delta/4\theta) \simeq 1. \tag{50}$$

For the present calculations the velocity profile in the computational domain is chosen to be

$$W(y^2) = \begin{cases} 1, & \gamma \le y^2 < y_i^2, \\ \frac{1}{2}\left\{1 + \tanh\left[\dfrac{B}{2\theta_B}\left(1 - \dfrac{f(b + \mathrm{i}y^2)}{f(b + \mathrm{i}y_o^2)}\right)\right]\right\}, & y_i^2 < y^2 < \infty, \end{cases} \tag{51}$$

where y_o^2 is the location of the half-velocity point, B is the length of the jet exit minor axis, θ_B is the momentum thickness on the minor axis, and y_i^2 is chosen such that

$$\tanh\left[\frac{B}{2\theta_B}\left(1-\frac{f(b+\mathrm{i}y_i^2)}{f(b+\mathrm{i}y_o^2)}\right)\right]\simeq 1. \tag{52}$$

The momentum thickness on the minor axis is defined by

$$\theta_B=\int_0^\infty W(0,x^2)[1-W(0,x^2)]\mathrm{d}x^2. \tag{53}$$

The choice of the constant b in equation (51) is arbitrary and $f(b+\mathrm{i}y_i^2)$ is defined by equations (8) and (10).

As an example consider the map,

$$f(y^1+\mathrm{i}y^2)=a\cos(y^1+\mathrm{i}y^2). \tag{54}$$

Then, with $b=\pi/2$, we obtain,

$$W(y^2)=\begin{cases}1, & \gamma\le y^2<y_i^2,\\ \frac{1}{2}\left\{1+\tanh\left[\dfrac{B}{2\theta_B}\left(1-\dfrac{\sinh(y^2)}{\sinh(y_o^2)}\right)\right]\right\}, & y_i^2<y^2<\infty.\end{cases} \tag{55}$$

This corresponds to the velocity profile used by Morris[8] to describe an elliptic jet. In this case it is readily shown that equations (53) and (55) are consistent if the condition (52) is satisfied. The solutions of the Rayleigh equation for velocity profiles of the form defined in this section are described next.

3. NUMERICAL RESULTS

In this section numerical solutions of the generalized Rayleigh equation are presented. Calculations are performed for the stability of jets with rectangular and elliptic mixing regions. The instability growth rates are determined for the varicose and flapping instabilities. The varicose mode is described by equation (40). It is even about both the jet's major and minor axes. The flapping mode is described by equation (41) and is odd about the major axis and even about the minor axis. Experiments have shown that these modes dominate the unsteady flow structure in elliptic and rectangular jets. As the jet Mach number increases, so the flapping mode becomes predominant. Examples of the eigenfunctions are also shown. To validate the numerical method, calculations are presented first for round and elliptic jets for which previous results have been obtained. For all the calculations shown, the Rayleigh equation is non-dimensionalized with respect to the jet exit mean velocity and static pressure and the jet's equivalent diameter.

3.1. Validation of the numerical method

The stability code has been validated numerically for several different geometries and boundary conditions. In the simplest check the generalized Rayleigh problem is reduced to the form of the model problem analysed in section 2.2. In this test the stability code reproduced exactly the error results exhibited in Table I.

The next series of numerical tests involves the calculation of the most unstable eigensolutions for the flapping and varicose instabilities of incompressible circular and elliptic jets. These calculations are

Table II. Comparison of present calculations for a circular jet with Morris[8] for an elliptic jet with aspect ratio $A/B = 1{\cdot}001$.

Mode	Frequency, ω	α_p	α_b	% Error
V	5·441	10·207 − 5·687i	10·199 − 5·685i	0·07
F_A	5·453	10·244 − 5·652i	10·238 − 5·649i	0·06
F_B	5·456	10·253 − 5·652i	10·243 − 5·651i	0·08

compared with those of Morris[8]. A relative error is introduced, defined by

$$\%\text{Error} = \frac{|\alpha_p - \alpha_b|}{|\alpha_b|} \times 100, \tag{56}$$

where α_p is the present result and α_b is taken from Morris[8]. For the circular jet case, a complex exponential map is used to generate the grid for the generalized Rayleigh problem. The mean velocity profile used in this computation is given by equation (49). In all the test cases the momentum thickness on the major axis, θ_A, was taken to be 0·02 as in Morris[8]. Also, as shown by Morris[8], for small momentum thicknesses and the velocity profile (51), $A\theta_A \simeq B\theta_B$, where A and B are the jet semi-major and semi-minor axes respectively. Finally, the boundaries of the computational domain are chosen such that

$$0{\cdot}001 \leq W \leq 0{\cdot}999 \tag{57}$$

Table II compares the eigenvalues computed with the present hybrid technique for the circular jet case with those of Morris[8] for an elliptic jet with aspect ratio $A/B = 1{\cdot}001$. In Table II F_A and F_B represent the modes flapping about the major and minor axes respectively and V represents the varicose mode. The present results are nearly independent of the number of collocation points in the azimuthal direction. This behaviour is expected because of the axisymmetry of the circular jet. In this case, the Runge–Kutta scheme uses a step size of 0·004 in the y^2 direction.

For the confocal elliptic jet test case (the mean velocity is constant along azimuthal co-ordinate lines in an elliptic cylindrical co-ordinate system) a complex cosine function is used to determine the computational grid. This transformation generates elliptic cylindrical co-ordinates in the physical plane. An aspect ratio, $A/B = 2$ elliptic shear layer has been considered. The mean velocity profile in this case is given by equation (55). Table III compares the present results obtained using the hybrid method with those of Morris[8]. A step size of 0.006 is used in the y^2 direction. 7 interior collocation points are used in the y^1 direction. If less than four interior collocation points are used, the calculated eigenvalues exhibit large errors. Conversely, if more than nine interior collocation points are used it becomes very difficult to isolate individual eigenvalues due to their close packing in the wavenumber plane for the test conditions. The addition of more interior collocation points to the computation affects two distinct limiting processes. First, the approximation of the eigenfunction

Table III. Comparison of present calculations for a elliptic jet of aspect ratio $A/B = 2{\cdot}0$ with Morris[8]

Mode	Frequency, ω	α_p	α_b	% Error
V	5·657	10·156 − 4·496i	10·135 − 4·507i	0·21
F_A	5·010	9·307 − 3·664i	9·322 − 3·667i	0·19
F_B	5·657	10·045 − 4·472i	10·027 − 4·507i	0·35

Table IV. Eigenvalues used in the circular jet eigenfunction calculations

Mode	Frequency, ω	α_p
V	5·44	10·20 − 5·68i
F_A	5·45	10·24 − 5·65i

becomes more accurate as more geometric information about the physical domain is supplied to the approximation. Second, the functions that define the boundary conditions on the edges of the shear layer become more accurate through the inclusion of terms that fluctuate more rapidly in the azimuthal direction. It is believed that the addition of these rapidly fluctuating terms leads to a determinant minimization problem that is ill-conditioned. Presently, this represents the major difficulty found in the use of the hybrid method for the solution of the Rayleigh problem. It should be noted that after these calculations were completed an error was detected in the high-order Bessel function routines. This may have led to the difficulty in obtaining convergence for a large number of interior points. However, no additional calculations have been performed as it is primarily the low order eigensolutions that are of interest.

As noted previously, the eigenfunction associated with a given eigenvalue may also be determined with the inverse interpolation method. Recall that in the present formulation the eigenfunctions correspond to the pressure fluctuation. All the other fluctuation quantities may be related to the pressure fluctuation and its derivatives. Thus, once the pressure eigenfunction is determined the distributions of the velocity components associated with the instability wave may also be found.

As a verification of the eigenfunction calculation technique, the eigenfunctions for the varicose (axisymmetric) and flapping (helical) modes of the circular jet have been calculated. The corresponding eigenvalues are given in Table IV. Contour plots of the real part of the eigenfunctions are shown in Figures 3 and 4. These plots present only the qualitative shape of the pressure field as the amplitude in the present linear analysis is arbitrary. For the varicose mode the amplitude and phase of the eigenfunction are constant along lines of constant radius. For the flapping mode, the amplitude is constant and the phase is equal to the azimuthal angle.

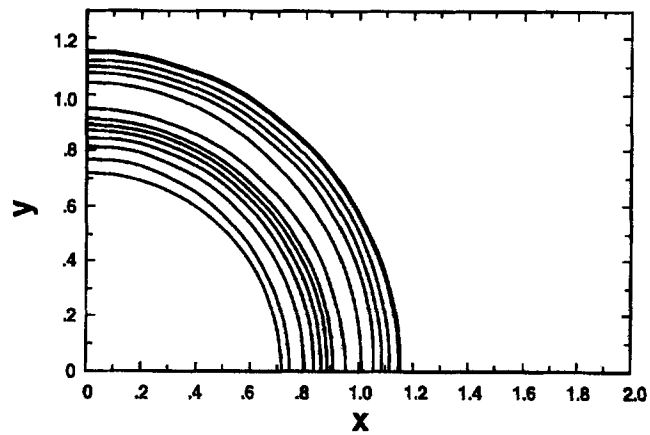

Figure 3. Iso-pressure contours for the varicose mode, V. Circular jet case. For eigenvalues see Table IV

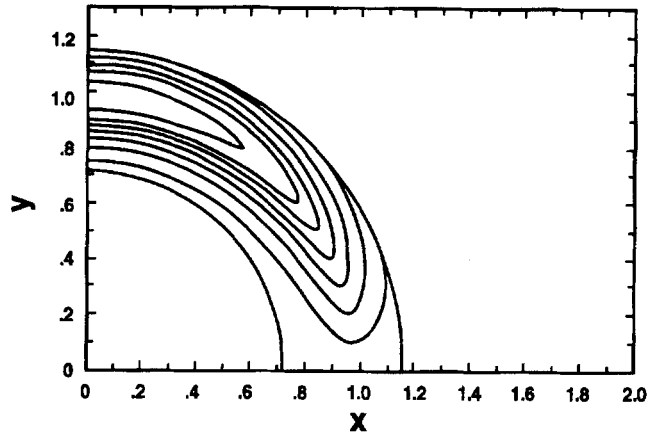

Figure 4. Iso-pressure contours for a flapping mode, F_A. Circular jet case. For eigenvalues see Table IV

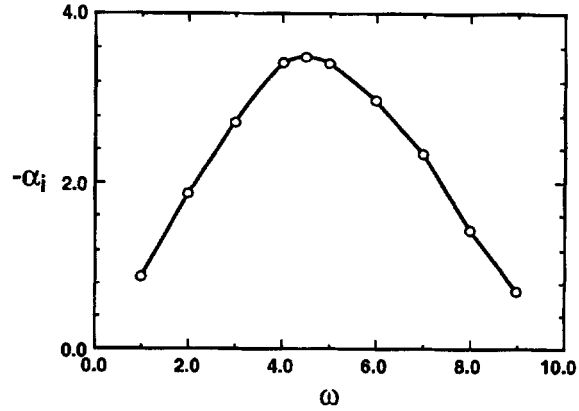

Figure 5. Variation of the axial growth rate as a function of frequency for the elliptic non-confocal jet of aspect ratio 2:1. Varicose mode, V

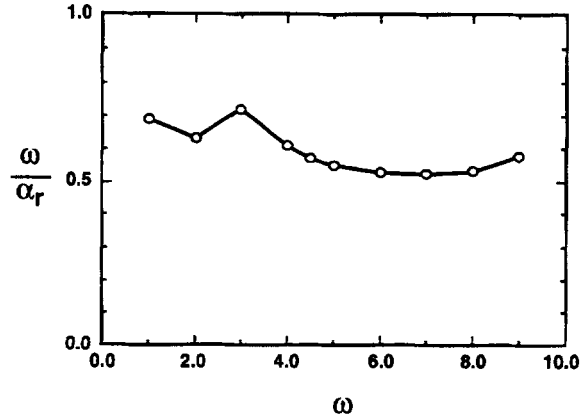

Figure 6. Variation of the phase velocity as a function of frequency for the elliptic non-confocal jet of aspect ratio 2:1. Varicose mode, V

3.2. *Elliptic and Rectangular Jet Stability Calculations*

As examples of the application of the hybrid method to more general problems than those treated in the previous section, non-confocal elliptic and rectangular jet shear layers have been considered. Both shear layers are defined such that the semi-major and semi-minor axes, A and B respectively, satisfy,

$$A/B = 2 \qquad \text{and} \qquad \sqrt{AB} = 1 \tag{58}$$

In addition, both jet shear layers are described by the hyperbolic tangent mean velocity profile given by equation (51). A constant momentum thickness in the computational plane of 0·02 is assumed in all the calculations. In the physical plane this results in a non-uniform azimuthal variation in the momentum thickness: the momentum thickness on the major axis being greater than that on the minor axis. This corresponds to the velocity profiles measured by Baty *et al.*[22] for an aspect ratio 2:1 elliptic, supersonic jet.

For the shear layers considered, the hybrid method used both 5 and 7 interior collocation points. The difference between the eigenvalues for these two choices was typically in the third or fourth significant figure. All the calculations for the elliptic shear layer were based on seven interior collocation points. Figure 5 shows the variation of the axial growth rate as a function of frequency for the varicose mode of the elliptic jet. The maximum growth rate is slightly lower than that determined for the confocal elliptic shear layer: see Table III. The variation of the phase velocity, defined by ω/α_r, for this case is shown in Figure 6 for the varicose mode. This result is typical of all the calculations for both the varicose and flapping instabilities in the elliptic and rectangular cases. For the varicose instability there is generally a slight decrease in the phase velocity at low frequencies. However, in all the cases considered, the phase velocities of the instability waves are approximately 60 per cent of the centreline velocity. These results are consistent with those of Koshigoe and Tubis[9,10]. To determine the most unstable mode the three largest growth rates were interpolated using a second order polynomial. Table V shows the frequencies for the maximum growth rates for this elliptic jet.

Figure 7 shows the variation of the axial growth rate as a function of frequency for the varicose mode of an aspect ratio 2:1 rectangular jet. The maximum growth rate is much lower than that for the elliptic jet. In addition, the frequency for the maximum growth rate is also reduced. Table VI shows the frequencies for the maximum growth rates for both the varicose and flapping instabilities. This frequency gives an indication of the initial vortex shedding frequency for the jet. The calculated reduction in this frequency for the rectangular jet could be due to either the change in the geometry or to the distribution of the momentum thickness around the jet.

As a final calculation we consider the pressure eigenfunctions for the elliptic and rectangular jets. Figure 8 shows the iso-pressure contours for the most unstable varicose instability in the elliptic jet and Figure 9 shows the corresponding contours in the rectangular jet case. As in the circular jet case the amplitude of the eigenfunctions is arbitrary. In Figures 8 and 9 the solid contours represent positive pressure fluctuations, while the dotted contours represent negative pressure fluctuations. The solid and dotted contours overlap on the zero pressure contour lines. The most notable feature in both figures is the apparent lack of uniformity, compared to the circular jet contours shown above. Very similar

Table V. Most unstable frequencies and wavenumbers for the non-confocal elliptic jet shear layer

Mode	Frequency, ω	α_p
V	4·49	7·86 − 3·50i
F_A	4·16	7·75 − 2·95i

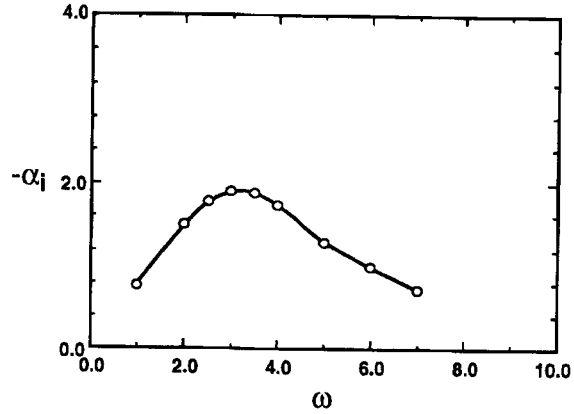

Figure 7. Variation of the axial growth rate as a function of frequency for the rectangular jet of aspect ratio 2:1. Varicose mode, V

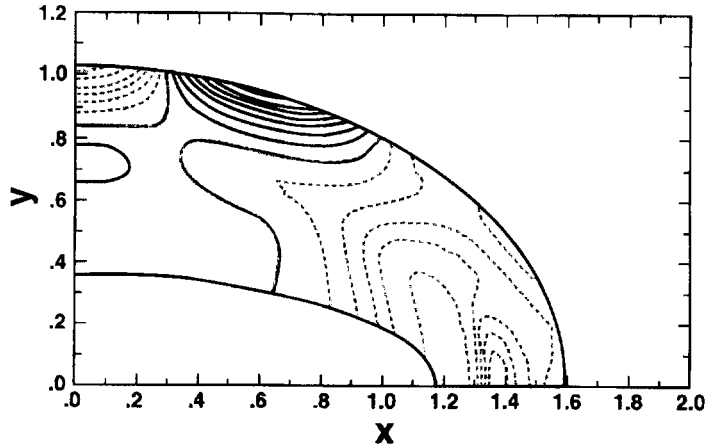

Figure 8. Iso-pressure contours for the elliptic non-confocal jet of aspect ratio 2:1. Varicose mode, V. For eigenvalues see Table V

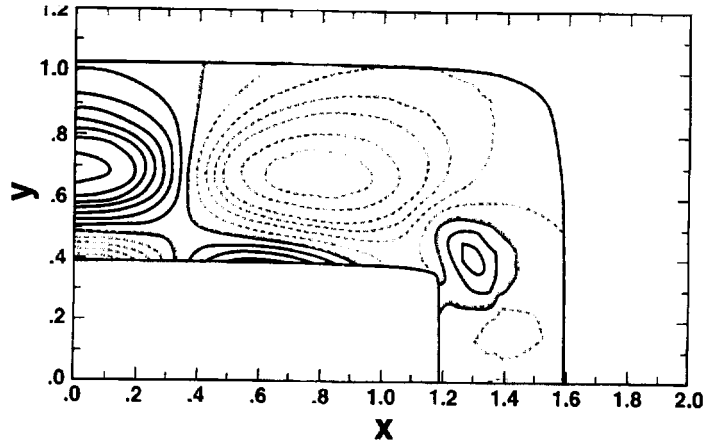

Figure 9. Iso-pressure contours for the rectangular jet of aspect ratio 2:1. Varicose mode, V. For eigenvalues see Table VI

Table VI. Most unstable frequencies and wavenumbers for the rectangular jet shear layer

Mode	Frequency, ω	α_p
V	3·16	5·71 − 1·92i
F_A	2·90	5·46 − 1·98i

distributions are found for the flapping modes so they are not shown here. Recent calculations by Tam and Thies[11] for a rectangular jet represented by a vortex sheet have shown that the instability modes may be classified into four symmetry types as discussed in this paper. In addition, they showed the existence of 'corner' and 'centre' modes. The former are isolated near the corners of the rectangular jet shear layer while the latter have their greatest fluctuations along the edges of the jet. Tam and Thies speculated that, for finite shear layer thickness, the 'centre' modes would dominate. Thus the present modes would likely be of this class. Though this is not immediately obvious from the pressure contours, this is not the case for the contours of equal Reynolds stresses and their gradients. In the rectangular jet case the distributions indicate that the jet is developing initially as two independent two-dimensional shear layers aligned along the jet's sides. However, in the elliptic jet case there is a continuous variation from the major to the minor axes with the dominant fluctuations, for the modes considered here being close to the major axis. Further details are given by Baty.[18]

4. CONCLUSIONS

This paper has presented a new calculation procedure to compute the eigenvalues and eigenfunctions of two-dimensional partial differential equations of the form given by equation (1). This calculation procedure, the hybrid scheme, has been used to analyse the spatial stability of jets of arbitrary exit geometry. Calculations have been performed for round, elliptic, and rectangular jets. Examples of the eigenvalues and eigenfunctions for the fluctuating pressure associated with the instability waves in these jets have been presented. The hybrid scheme yielded very good results for both a model problem and benchmark jet stability problems. All the calculations presented here have considered incompressible jets. Compressible flow cases are a simple extension of the present work and examples for the compressible case are given by Baty *et al.*[22]

For the non-circular jet stability calculations considered here, conformal maps have been used to carry standard computational domains onto realistic jet cross sections. However, the hybrid numerical scheme does not depend on the use of conformal maps. For non-circular jets in which the conformal maps are not known or difficult to compute, standard two-dimensional grid generation methods may be applied to determine the necessary co-ordinate transformations. The use of such transformations would require that the Rayleigh equation be developed for metric tensors that have non-zero off-diagonal terms.

It is possible that further improvements in computer time and robustness could be achieved if the analytical solutions at the boundaries of the computational domain were written in a more natural co-ordinate system. For example, Morris[24] used elliptic cylindrical co-ordinates and wrote the analytic solutions in terms of Mathieu and modified Mathieu functions. It was found that very few terms in the series representation were then needed to obtain accurate eigenvalues. This suggests that fewer interior collocation points would be needed in the hybrid method presented here to achieve the same level of accuracy.

Once the fluctuating pressure is computed from the Rayleigh equation, the fluctuating velocity components may be obtained using the linearized equations of continuity and momentum. In turn, this

enables the second-order statistics, including the normal and shear stresses, associated with the instability waves to be calculated. If it is argued that the mixing process in free shear flows is dominated by large scale structures and that, locally, they may be modeled as instability waves, these second-order statistics are all that is needed to provide a turbulence closure scheme. Such turbulence models have been developed by Morris *et al.*[5] and Liou and Morris[6] for a two-dimensional shear layer and by Viswanathan and Morris[23] for a circular jet. The encouraging results of these turbulence models suggest that the present hybrid numerical method could be used to develop turbulence closure schemes for jets with arbitrary exit geometries.

ACKNOWLEDGEMENTS

This work was supported by NASA Langley Research Center under NASA Grant NAG-1-657. The technical monitor was Dr J. M. Seiner.

REFERENCES

1. M. Gaster, E. Kit, and I. Wygnanski, 'Large-scale structures in a forced turbulent mixing layer', *J. Fluid Mech.* **150**, 23–39 (1985).
2. R. A. Petersen and M. M. Samet, 'On the preferred mode of jet instability', *J. Fluid Mech.* **194**, 153–173 (1988).
3. C. K. W. Tam and P. J. Morris, 'The radiation of sound by the instability waves of a compressible plane turbulent shear layer', *J. Fluid Mech.* **98**(2), 349–381 (1980).
4. C. K. W. Tam and P. J. Morris, 'Tone excited jets, Part V: A theoretical model and comparison with experiment', *J. Sound Vib.* **102**(1), 119–151 (1985).
5. P. J. Morris, M. G. Giridharan and G. M. Lilley, 'On the turbulent mixing of compressible free shear layers', *Proc. Roy. Soc. Lond.* **A 431**, 219–243 (1990).
6. W. W. Liou and P. J. Morris, 'Weakly non-linear models for turbulent mixing in a plane shear layer', *Phys. Fluids, A* **4**(12), 2798–2808 (1992).
7. E. Gutmark, K. C. Schadow and K. J. Wilson, 'Noncircular jet dynamics in supersonic combustion', *J. Prop. Power* **5**(5), 529–533 (1989).
8. P. J. Morris, 'Instability of elliptic jets', *AIAA J.* **26**(2), 172–178 (1988).
9. S. Koshigoe and A. Tubis, 'Wave structures in jets of arbitrary shape. I. Linear inviscid spatial instability analysis', *Phys. Fluids* **29**(12), 3982–3992 (1986).
10. S. Koshigoe and A. Tubis, 'Wave structures in jets of arbitrary shape. II. Application of a generalized shooting method to linear instability analysis', *Phys. Fluids* **30**(6), 1715–1723 (1987).
11. C. K. W. Tam and A. T. Thies, 'Instability of rectangular jets', *J. Fluid Mech.* **248**, 425–448 (1993).
12. W. S. Saric, and A. H. Nayfeh, 'Nonparallel stability of boundary-layer flows', *Phys. Fluids* **18**(8), 945–950 (1975).
13. R. Wegmann, 'An iterative method for conformal mapping', in *Numerical conformal mapping*, ed. L. N. Trefethen, North-Holland, pp. 7–18, 1986.
14. R. Wegmann, 'An iterative method for conformal mapping of doubly connected regions', in *Numerical conformal mapping*, ed. L. N. Trefethen, North-Holland, pp. 79–98, 1986.
15. R. Wegmann, 'Convergence proofs and error estimates for an iterative method for conformal mapping', *Numer. Math.* **44**, 435–446 (1986).
16. L. N. Trefethen, 'Numerical computation of the Schwartz-Christoffel transformation', *SIAM J. Sci. Stat. Comp.* **1** , 82–102 (1980).
17. L. N. Trefethen, 'SCPACK user's guide', *ICASE Internal Report No.* 24 (1983).
18. R. S. Baty, *Reynolds stress closure in jet flows using instability wave modeling*, Ph.D. thesis, Aerospace Engineering, The Pennsylvania State University, 1989.
19. R. G. Voigt, D. Gottlieb and M. Y. Hussaini, *Spectral Methods for Partial Differential Equations*. SIAM, Philadelphia, 1984.
20. G. W. Stewart, *Introduction to matrix computations*. Academic Press, London, 1973.
21. A. Michalke, 'Instabilitat eines kompressiblen runden Freistrahls unter Berucksichtigung des Einflusses der Strahlgrenzschichtdicke', *Z. Flugwiss.* **19**, 319–328 (1971).
22. R. S. Baty, J. M. Seiner and M. K. Ponton, 'Instability of a shock-free elliptic jet', *AIAA Paper No.* 90–3959 (1990).
23. K. Viswanathan and P. J. Morris, 'Predictions of turbulent mixing in axisymmetric compressible shear layers', *AIAA J.* **30**(6), 1529–1536 (1992).
24. P. J. Morris, 'The spatial stability of compressible elliptic jets', *Phys. Fluids* **7**(1), 185–194 (1995).